SAND2022-7270J

ARTICLE

Tuneable Phase Behaviour and Glass Transition via Polymerization-Induced Phase Separation in Crosslinked Step-Growth Polymers

Received 00th January 20xx,
Accepted 00th January 20xx

DOI: 10.1039/x0xx00000x

Samuel C. Leguizamon,[a] Juhong Ahn,[b] Sangwoo Lee,[b] and Brad H. Jones [a]*

Once limited to chain-growth polymerizations, fine control over polymerization-induced phase separation (PIPS) has recently been demonstrated in rubber-toughened thermoset materials formed through step-growth polymerizations. The domain length scales of these thermoset materials can be elegantly tuned by utilizing a binary mixture of curing agents (CAs) that individually yield disparate morphologies. Importantly, varying the composition of the binary mixture affects characteristics of the materials such as glass transition temperature and tensile behavior. Here, we establish a full phase diagram of PIPS in a rubber-toughened epoxy system tuned by a binary CA mixture to provide a robust framework of phase behaviour. X-ray scattering *in situ* and post-PIPS is employed to elucidate the PIPS mechanism whereby an initial polymerization-induced compositional fluctuation causes nanoscale phase separation of rubber and epoxy components prior to local chain crosslinking and potential macrophase separation. We further demonstrate the universality of this approach by alternatively employing binary epoxy or binary rubber mixtures to achieve broad variations in morphology and glass transitions.

1. Introduction

Polymerization-induced phase separation (PIPS) is a simple method to introduce periodic structure in linear and crosslinked polymers at length scales ranging from several nm to several μm.[1-8] A multi-component, reactive mixture that is initially a single homogeneous phase is entropically driven to separate into chemically distinct phases, due to the increase in molecular weight associated with polymerization of one or more components. PIPS has been used to improve the properties of crosslinked polymers and to create unique functional microstructures, thereby opening new applications for such materials.[9-16] When employed with rubbers (*i.e.*, polymers with low glass transition temperature, T_g), PIPS generates rubber domains capable of increasing the energy required for a crack to propagate through an otherwise brittle, highly crosslinked polymer.[17-23] PIPS has also been used to generate porous 3D structures and membranes,[6, 24, 25] electrolytes,[26-28] and even bio-inspired metamaterials.[15, 29, 30]

The ability to control morphology and, in particular, the length scale over which PIPS occurs is critical where applications are concerned. To give several examples, the toughening effect of a rubber, the transport properties of a porous membrane or electrolyte, and the optical response of a metamaterial are all strongly dictated by the size, density, and inter-connectivity of phase-separated domains.[6, 24, 25, 31-35] Thus, recent work in PIPS has focused on tuneability – manipulating the chemistry of the initial mixture to achieve controlled final structures[4, 8, 12, 36]. The use of block copolymers has been particularly instrumental in the tuning of microstructures to achieve increases in Young's modulus, tensile strength, and elongation at break.[1, 2, 37, 38] However, PIPS has been historically difficult to control in crosslinked polymers generated from step-growth polycondensation reactions, such as epoxies, polyurethanes, and polyesters, which are widely used as adhesives, as structural matrices for composites, and in electronic components, on account of their thermal and chemical stability and rigidity.

Very recently, we introduced an elegantly simple approach to tune PIPS morphology over nanoscale to macroscale dimensions in rubber-toughened epoxy resin crosslinked with common diamine curing agents (CAs).[39] We showed that two different CAs can be selected to yield extremely disparate phase-separated length scales based on their chemical structure or reactivity. Then, the morphology can be conveniently tuned between these extremes by employing a binary mixture of the CAs, with their relative ratio dictating the final structure. In addition, we found that key physical properties, such as the breadth and position of T_g, varied in a remarkably complex manner with the CA composition, and we

[a] *Department of Organic Materials Science, Sandia National Laboratories, Albuquerque, NM, 87185, USA*
[b] *Department of Chemical and Biological Engineering, Rensselaer Polytechnic Institute, Troy, NY, 12180, USA*
Electronic Supplementary Information (ESI) available: [details of any supplementary information available should be included here]. See DOI: 10.1039/x0xx00000x

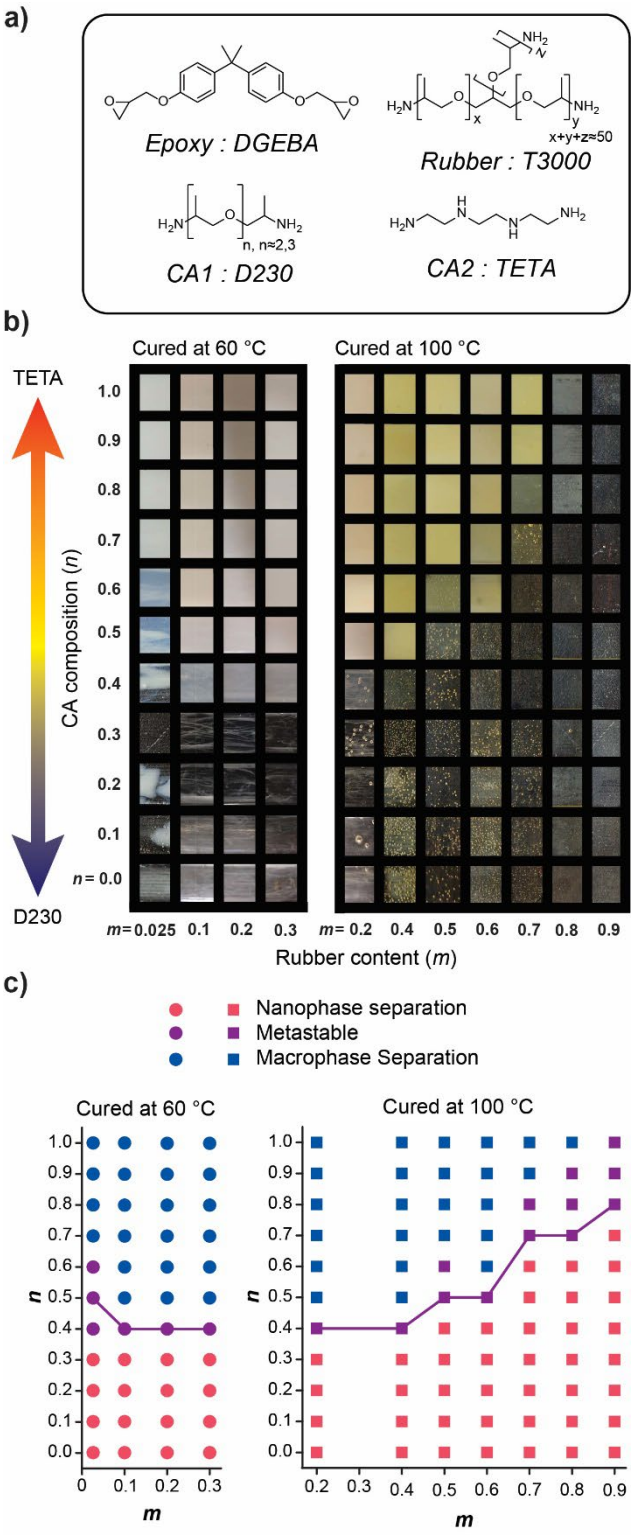

Figure 1. Tunable PIPS in an epoxy thermoset using a binary curing agent (CA) mixture and a rubbery polymer. (a) Chemical structures of DGEBA, T3000, D230, and TETA. (b) Images of epoxy plaques on black background. Plaques are made by varying CA composition n (n=[−NH−]$_{0,TETA}$/([−NH−]$_{0,TETA}$+[−NH−]$_{0,D230}$) and rubber content m (m=[−NH−]$_{0,T3000}$/[−NH−]$_{0,total}$) and curing at 60°C or 100°C. Note that bubbles are present in many samples and should not be confused with opacity. (c) Phase diagrams of the CA-tuned system.

illustrated how this newly discovered tuneability could be used to optimize useful characteristics of the material such as tensile behaviour.

A particularly exciting aspect of this approach is its potential universality. We anticipate that PIPS can be precisely controlled in all step-growth polymers to develop new materials with targeted structures and functionalities, as well as unconventional and/or improved thermomechanical, transport, and optical properties, provided a robust framework of phase behaviour and structure-property relationships is established. With these considerations in mind, here we expand upon the limited scope of our initial work to establish a full phase-diagram for a tuned, rubber-toughened epoxy. We utilize time-resolved X-ray scattering to further understand the mechanism by which PIPS occurs in these systems. Moreover, we demonstrate that PIPS tuneability is not limited to binary CA mixtures, but can additionally be attained through binary epoxy or rubber mixtures with a single CA thus generating a diverse range of desired material properties, as exemplified by the glass transition.

2. Results and Discussion

Previously, diglycidyl ether of bisphenol A (DGEBA) was used as the epoxy resin, Jeffamine T3000 (a commercial amine-terminated polyether) was used as a reactive, amine-functionalized rubber, while triethylenetetramine (TETA) and Jeffamine D230 were used as incompatible and compatible CAs, respectively, for the binary mixture (Figure 1a).[39] The system can be tuned through the parameters of rubber content and the composition of the CA mixture defined by the variables m and n, respectively. Here, increasing values of m indicate higher rubber content (m=0 is entirely epoxy + CA, m=1 is entirely rubber), whereas increasing values of n indicate increased TETA content and decreased D230 content within the binary CA mixture (n=0 the CA is pure D230, n=1 the CA is pure TETA). For a further detailed definition of these parameters refer to the full experimental procedures in the Supplementary Information. As the chemically identical backbones of D230 CA and T3000 rubber enhance compatibility of the rubber and epoxy matrix, while the dissimilar TETA CA favors phase separation, low n yields nanophase separation, while high n yields macrophase separation. As demonstrated in our previous work, the boundary between nanophase and macrophase separation is readily apparent by both a visual transition in samples from transparent to opaque and a transition from a single, broad glass transition to two well-resolved ones. Given our initial focus on rubber toughening and mechanical properties, the previous study was limited to samples with m≤0.3 (< about 40 wt% T3000). Here, we first investigated the full phase diagram of the original system to obtain a deeper understanding of PIPS in CA-tuned epoxies.

As mentioned, visual observation of the CA-tuned epoxies can be used to roughly delineate their phase separated structures. Transparent materials consist of either a single, homogeneous phase, or instead are nanophase separated, whereas opaque

materials are macrophase separated (Figure 1b). For each value of *m,* samples with a blue-tinted, cloudy appearance were observed intermediate to the transparent and opaque regimes (e.g., Figure 1b m=0.025 and 0.4≤n≤0.6). This bluish tint indicates that the characteristic length scale of the phase separated structure was approaches the visible light regime.[29] We previously identified this phase separation as a kinetically metastable state whereby the network morphology is arrested during the course of the polymerization. This phenomenon is commonly seen in thermally quenched systems.[40-42] Qualitatively, we found little effect of cure temperature on the ultimate phase separated structure in comparison to the effect of CA composition and rubber content. This fact is exemplified by the data shown for m=0.2, where the metastable state persists at n=0.4 when cured at either 60 °C or 100 °C. On the other hand, the temporal evolution of the phase separated structure depends strongly on cure temperature, as seen in time-resolved X-ray scattering measurements discussed shortly.

We believe the phase behaviour in these materials is primarily dictated by the extent to which the separating components are covalently linked, with fewer linkages between incompatible components leading to macrophase separation, i.e, more homogeneous chain domains. A schematic illustration is provided in Figure S1. This hypothesis is based on the expectation that segregation strength, dictated by χN where χ is the interaction parameter and N is the degree of polymerization, should increase as the binary CA and rubber become less chemically distinct (meaning more TETA and less D230 in this case). Consistent with the hypothesis, Figure 1b indicates that more TETA (higher n) was required to observe macrophase separation with larger rubber loadings (m). Both the rubber and the CAs are reactive with the epoxy resin. With larger m, a greater fraction of covalent bonds between the resin and rubber should be expected at the onset of PIPS. Thus, a larger degree of incompatibility is needed in the binary CA mixture to induce macrophase separation. The CA composition n corresponding to the onset of macrophase separation increases monotonically from m=0.1 until no macrophase separation is observed at m=0.9. The metastable region similarly shifts with m and occurs with a minimum value of n=0.4 at 0.1≤m≤0.3. Interestingly, the range of n for the metastable domain slightly increases at the extremes of m, suggesting a critical point at n ≈ 0.4 and m ≈ 0.2 from which the metastable domain enclosed by spinodal and binodal curves progressively enlarges as the system moves away from the critical point. As suggested previously, these observations further draw a parallel with the temperature-dependent phase diagram of a two-component polymer blend given by Flory-Huggins solution theory.[43-46] However, here, wide metastable windows at compositional extremes are observed as χ is varied based on chemical compatibility (through n) likely due to the weak temperature dependence of χ. Mixtures that begin further from the boundary for phase separation exhibit nanoscale morphologies while mixtures closer to the boundary exhibit macroscale morphologies (Figure S1). Mixtures further from the boundary will possess a greater number of covalent linkages between epoxy and rubber when the boundary is crossed, thus favoring the formation of phases with smaller length scales.

For more precise analysis regarding the phase behaviour and network structure of the thermosets, the composition space was investigated using small- and wide-angle X-ray scattering (SWAXS) characterization. The representative SWAXS patterns of samples at m = 0.3 are presented in Figure 2 and reveal several broad scattering features; $q_{x\text{-}link}$, q_m, and q_l located at approximately 0.3 Å^{-1}, 0.06 Å^{-1}, and 0.01 Å^{-1} respectively. Those characteristic reciprocal lengths are identified by comparing the scattering patterns of cured thermosets and starting materials summarized in Figure 2. We note that the scattering features at q > 1 Å^{-1} represent the inter- and intra-correlations of molecular functional groups as previously described for another polymer system.[47] It was previously determined that $q_{x\text{-}link}$ peaks ($d_{x\text{-}link}$=1.38 – 1.57 nm) were associated with the crosslink lengths of the CA-crosslinked epoxy while q_l and q_m describe the complex length scale of the rubber and the strong nanoscale variations in composition between epoxy and rubber domains, with q_m indicating a peak value and q_l indicating the heterogeneity in this length scale.[39] For a given series of n at constant m, the longest wavelength, d_l, of the nanoscale structure increased up to the value of n at which metastability is observed, for example, n = 0.4 in Figure 2a, and then decreased at higher values. Similarly, the scattering intensities of the q_m domain had a maximum at the metastable value, and therefore the domains also had the largest compositional differences at these values of n (Figure 2b and S2). In the metastable and macrophase separated regimes, new features are evident at very low q < 0.001 Å^{-1} that can be attributed to the formation of larger, micron-sized epoxy and rubber domains. As one progresses deeper into the macrophase separated regime (larger n), the macroscale structure becomes dominant at the expense of the nanoscale. Values for q_l, q_m, and $q_{x\text{-}link}$ are given for each series in Tables S2-4, respectively.

X-ray scattering characterization of the thermoset system was conducted over the time, composition, and curing temperature parameters for holistic understanding of the nanoscale structures of the thermosets. The time-resolved X-ray scattering characterization was conducted at m=0.3 and n=0.5 which is located in the macrophase separated regime, yet with a strong signature of scattering from nanodomains. The scattering patterns of pure starting compounds and the mixture of amine CAs displayed correlation peaks only in the wide-angle X-ray scattering (WAXS) domain (q > 1 Å^{-1}) of the segmental spatial relationships, as well as universal upturn features in the small-angle X-ray scattering (SAXS) domain (q < 0.02 Å^{-1}) (Figure 2c). The flat baseline intensity profiles in the medium-angle X-ray scattering domain (MAXS, 0.02 Å^{-1} < q < 1 Å^{-1}) of those starting materials show that no notable structural feature exists in this length scale, d_{MAXS} = 1 – 30 nm.[47] However, the X-ray scattering of the initial mixture of DGEBA and amine CAs at 25 °C, which is not yet cured, revealed scattering features corresponding to the length $d_l = 2\pi/q_l$ = 60 nm to $d_{x\text{-}link} = 2\pi/q_h$ = 2 nm with $d_m = 2\pi/q_m$ = 12.7 nm (Figure 2c). This observation

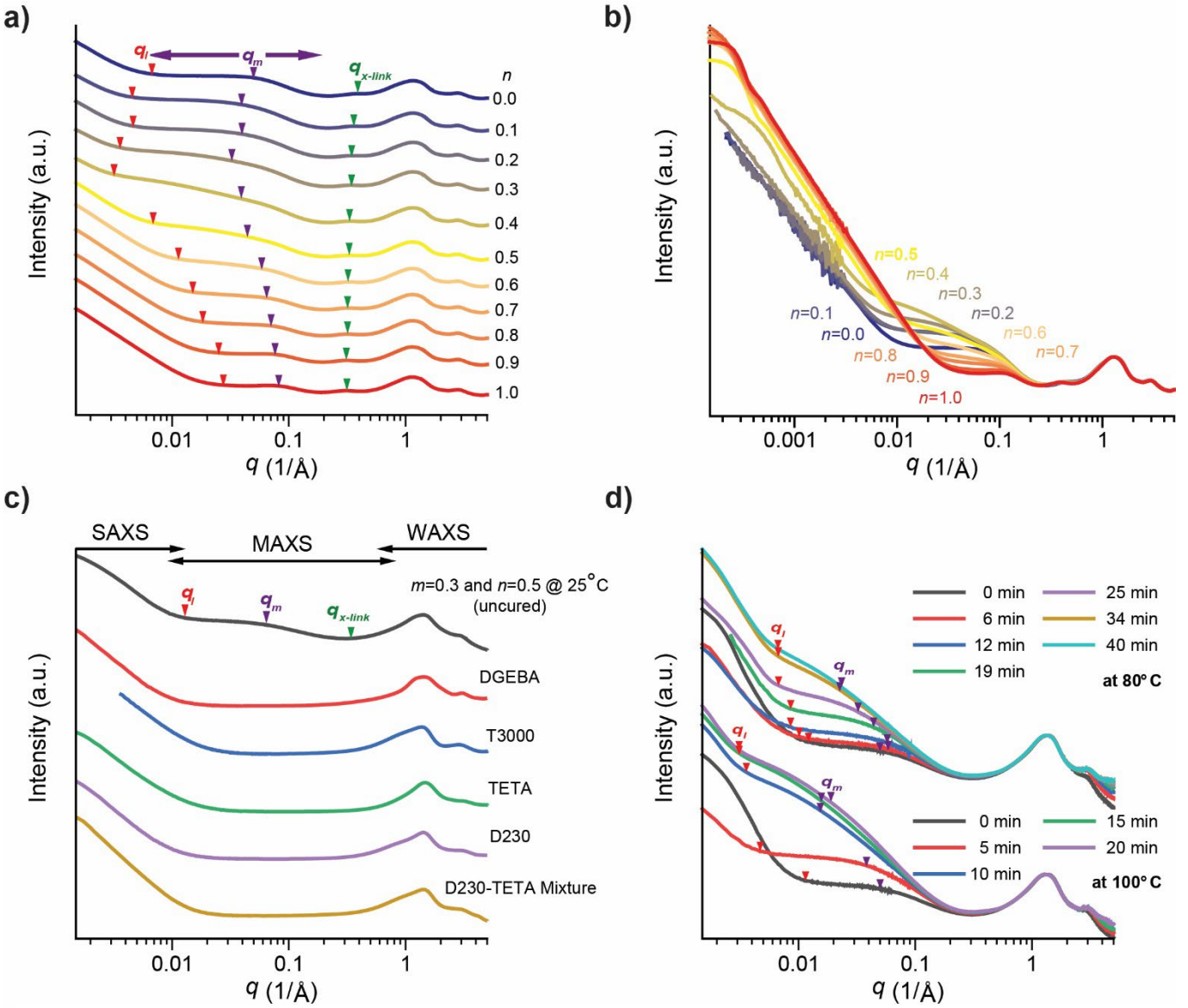

Figure 2. X-ray scattering of CA-tuned epoxies. (a) SWAXS patterns and (b) overlaid SWAXS patterns of samples with m = 0.3. (c) SWAXS patterns of the starting materials and the mixture before curing and (d) of the time-resolved experiments of the system at m = 0.3 and n = 0.5 at 80 °C and 100 °C.

reveals that the freshly mixed epoxy, CAs, and rubber are already in close proximity to a phase boundary and the domains are exhibiting significant composition fluctuations by nanoscale aggregates, *i.e.*, local, spatial variation in composition, between the unreacted liquid constituents, as observed from other systems in the vicinity of the phase boundary.[48-50~~51~~]

During cure at elevated temperatures, the mixture developed enlarging and amplifying compositional fluctuations as shown by the decreasing $q_I \sim d_I^{-1}$ and increasing scattering intensity (Figure 2d). The scattering profiles of the mixture nearly saturated at 40 mins with the $d_I \approx 108$ nm and $d_m \approx 27.4$ nm for 80 °C and at 20 mins with $d_I \approx 210$ nm and $d_m \approx 35.5$ nm for 100 °C. We also observed that the scattering intensity of the saturated q_m domain of the mixture cured at 100 °C is larger than that of the mixture at 80 °C. Those observations show that the compositional fluctuation in the mixture intensifies as the curing (polymerization) proceeds, i.e., less epoxy in aggregated rubber domains and *vice versa*, and the wavelength of the fluctuation ($d_m \sim q_m^{-1}$) is proportional to temperature. Additionally, the higher scattering intensity at 100 °C suggests a larger degree of the compositional contrast in the nanophase-separated domains as the scattering intensity $I \sim \Delta\rho$ where $\Delta\rho$ is the electron density difference of domains proportional to the difference of chemical compositions. However, over the period of the time-resolved scattering measurements, the correlation peaks of the CA-crosslinked epoxy, which conventionally appears at $q_{x\text{-link}} \approx 0.4$ Å^{-1} = 2π/1.6 nm in fully cured samples as exemplified in Figure 2a, did not develop. This behaviour suggests that the nanoscale phase segregation between the rubber and epoxy components proceeds first *via* polymerization-induced compositional fluctuation, yet additional local chain crosslinking is subsequently necessary to observe the $q_{x\text{-link}}$ peaks characteristic of the epoxy-CA component of the network.[52]

The phase behaviour, coupled with the relative fraction of the phases, strongly affects the macroscopic glass transition of

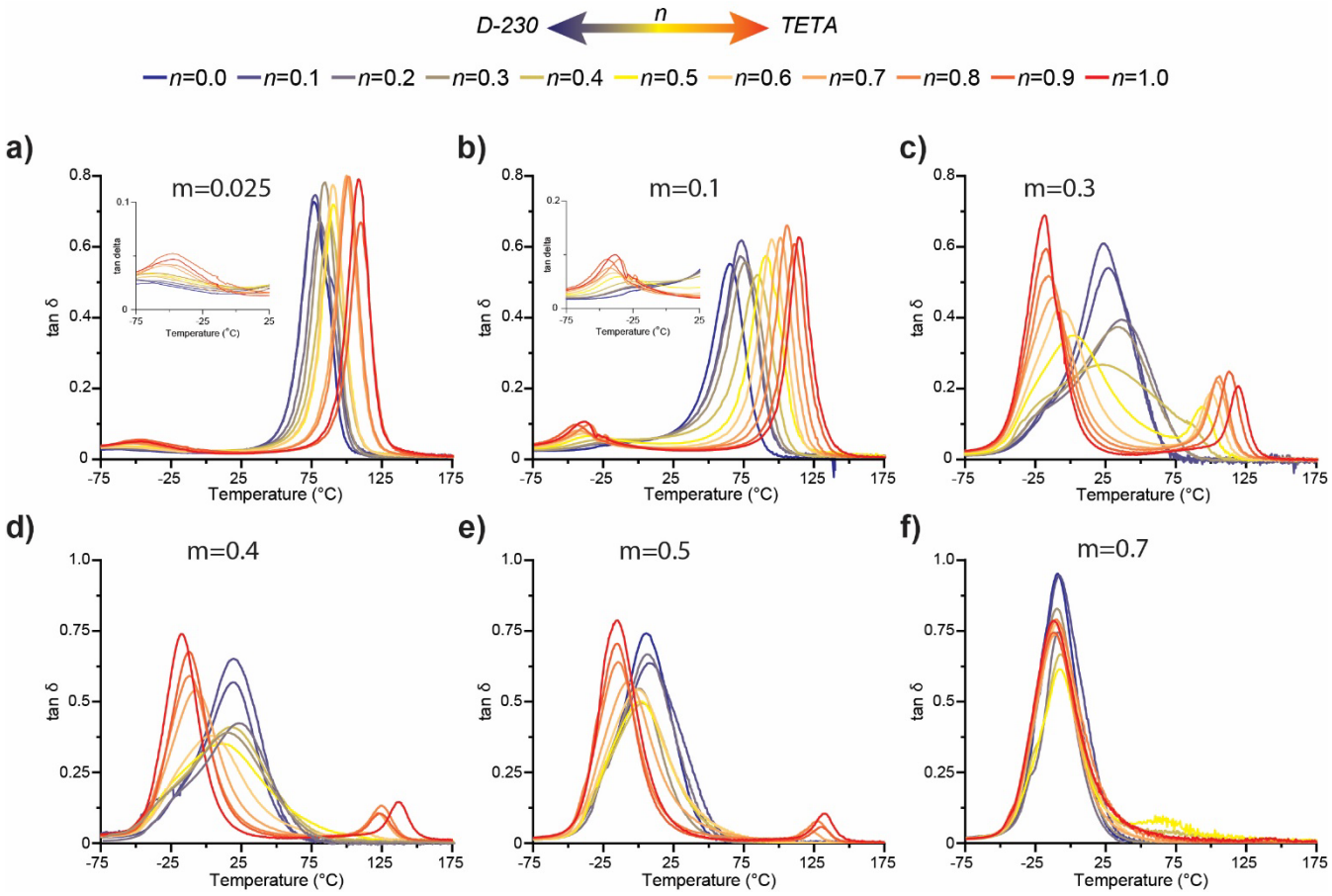

Figure 3. Loss tangent vs. temperature CA-tuned epoxies cured at 60°C or 100°C with variable rubber content (*m*) and curing agent composition *n*=0-1.0; (a) *m*=0.025, (b) *m*=0.1, (c) *m*=0.3, (d) *m*=0.4, (e) *m*=0.5, (f) *m*=0.7. Samples with *m* values of 0.025, 0.1, and 0.3 were cured at 60°C and samples with *m* values of 0.4, 0.5, and 0.7 were cured at 100°C.

these materials. Therefore, dynamic mechanical analysis (DMA) was employed to investigate the extent to which the glass transition can be tuned using the broad parameter space afforded by our approach (Figure 3 and S2).[53, 54] The opaque, macrophase separated materials always exhibit two local maxima in the loss tangent measured as a function of temperature. The relative strength of these individual relaxations scales with *m*, such that the high and low temperature relaxations can be unequivocally ascribed to the glass transitions of the epoxy-rich and rubber-rich domains, respectively. There is little dynamic heterogeneity in the macrophase separated regime; indeed, the individual relaxations trend towards the T_gs of pure CA-crosslinked epoxy and pure rubber as one progresses deeper into this regime. In contrast, the nanophase separated and metastable materials always exhibit a single maximum in the loss tangent. The overall glass transition in these regimes can instead be considered as a mixing of the individual relaxations. At low *m*, the glass transition is similar to pure CA-crosslinked epoxy, and the effect of the rubber is essentially to reduce T_g. Similarly, at high *m*, the glass transition is similar to pure rubber, and the effect of the epoxy is essentially to increase T_g. However, when there are similar amounts of rubber and epoxy, such as at *m*=0.3 and *m*=0.4, the glass transition is intermediate to the two extremes, and broadens substantially, indicating a high degree of dynamic heterogeneity. The breadth of the glass transition can be tuned by the CA composition, with the broadest T_g occurring in the metastable regime. This ability to tune the glass transition breadth may have practical implications for applications of crosslinked step-growth polymers. Good vibration damping requires a high loss factor at the frequency of interest, thus broad glass transitions give better damping performance over a wider range of frequency and temperature.[55] Networks with dynamic heterogeneity can also be cured at lower temperatures than their homogeneous counterparts, due to residual molecular mobility associated with vitrified networks that possess a broad glass transition.[52, 56]

Having established the broadly tunable phase behaviour and glass transitions via PIPS with a binary CA mixture, we hypothesized that a similar approach could be used with a binary epoxy or rubber mixture where each component of each mixture could be chosen to favor or oppose phase separation. Given that T3000 rubber strongly phase separates from TETA-crosslinked DGEBA, DER (an epoxy-functionalized propylene glycol oligomer) was chosen as an alternative epoxy resin. As anticipated given the identical backbones of DER and T3000, samples made from exclusively DER, T3000, and TETA (*m*=0.1) produced a transparent material as opposed to the opaque material using DGEBA as the epoxy. Thus, a new parameter, *e,*

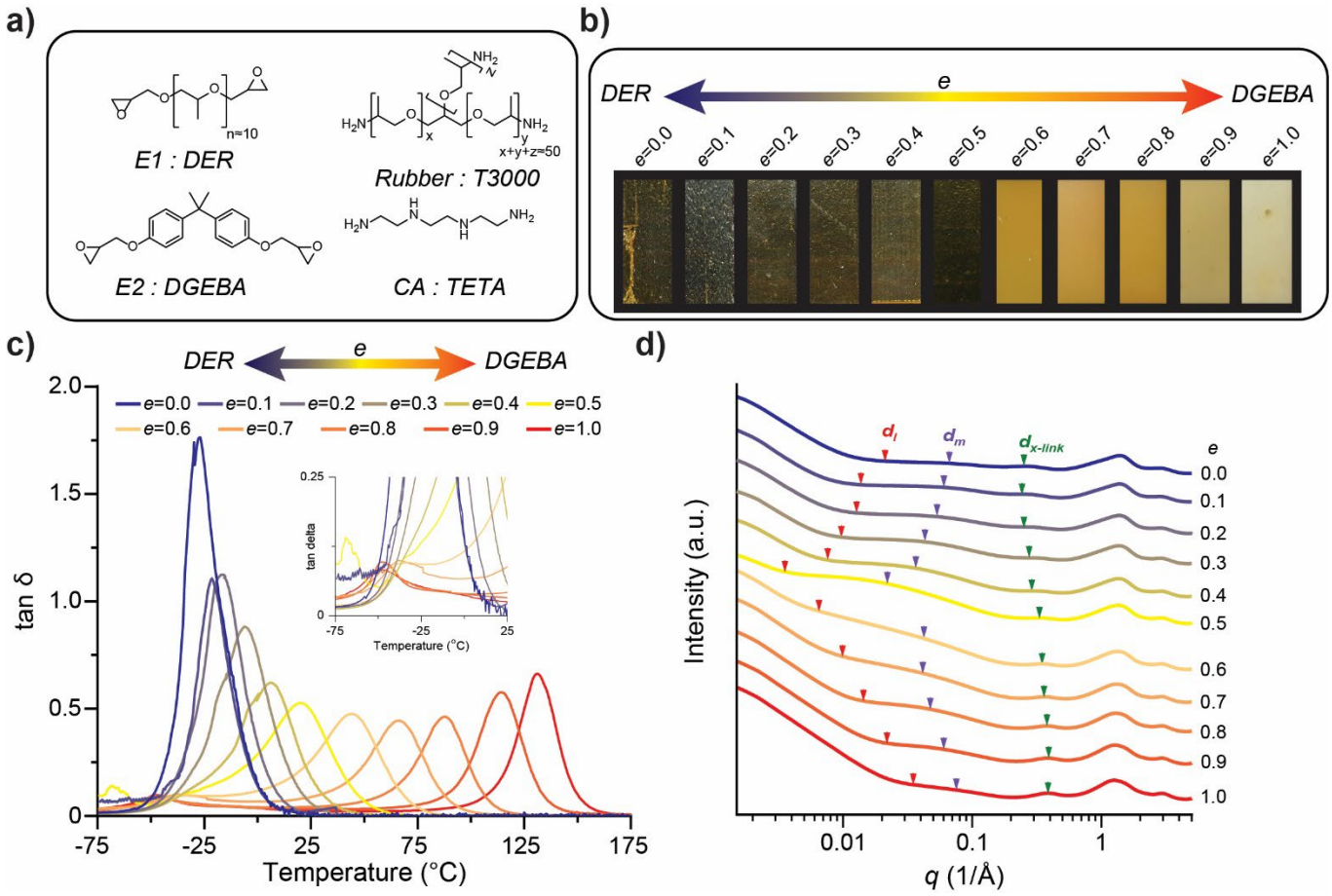

Figure 4. Tunable PIPS by exploiting a binary epoxy resin mixture. (a) Chemical structures of DGEBA, DER, T3000, and TETA. (b) Images of plaques, (c) loss tangent vs. temperature, and (d) SWAXS patterns for resin-tuned epoxies with m=0.1 and varied e.

for a binary epoxy mixture composition was defined where e=0 and e=1 correspond to entirely DER and entirely DGEBA, respectively (Figure 4). A rubber loading of m=0.1 was used to assess the new parameter's ability to tune morphology and glass transition in a rubber-toughened epoxy system as our previous work demonstrated values of m greater than 0.2 resulted in a rubber-rich continuous matrix and CA-rich dispersed domains.[39] This inversion of matrix/domain composition as compared with m≤0.1 yielded significant loss in mechanical properties. Transparent samples were observed at values of e below 0.5, where DER comprised the majority of the binary mixture, but opaque samples were produced at values of 0.5 and greater (Figure 4b). Interestingly, no plaques were observed with the cloudy appearances indicative of metastable morphologies. The SWAXS patterns of the resin-tuned materials (Figure 4d) mirrored the CA-tuned materials, with features q_l and q_m arising from nanoscale domains that varied significantly in position as the composition was tuned, as well as the feature $q_{x\text{-link}}$ corresponding to the crosslink length of the epoxy. Again, the largest length scales of nanodomains d_l and d_m were observed at the onset of the macrophase separated regime. At the extremes of the series, e=0 and e=1, the nanoscale structure q_m is nearly suppressed, and this indicates that the compositional fluctuations at those terminal compositions are very weak. The crosslink length $d_{x\text{-link}}$ shows significant variation as the resin is tuned, in contrast to the CA-tuned materials (Table S5). This variation reflects the decreased crosslink density of a DER-based epoxy compared to a DGEBA-based epoxy.

As before, the opaque, macrophase separated materials exhibited loss tangents with two local maxima at e≥0.6, merging into a single, broad T_g at higher DER content (Figure 4c). The inset in Figure 4c shows the loss tangent at low temperatures, where there is a weak relaxation between -75 and -25 °C in the materials with e>0.6 which can be attributed to the macrophase separated rubber domains. Interestingly, tuning e created rapid changes in the glass transition of the system in the macrophase separated regime and resulted in an increased range of accessible, broad T_gs as opposed to the CA-tuned system. Unlike the CA-tuned system, where variations in CA composition have little impact on the glass transition of the epoxy domains, here, the TETA-crosslinked DER has a much lower T_g than TETA-crosslinked DGEBA. Thus, the tuning effect of DER is to lower the T_g of the epoxy domains by reducing their crosslink density, as well as to merge the individual relaxations of the epoxy and rubber domains through the phase behaviour. As in the CA-tuned system, the breadth of the glass transition can be tuned by the resin composition, with the broadest T_g occurring near the boundary between nanophase separation and macrophase separation, where nanoscale compositional fluctuations are

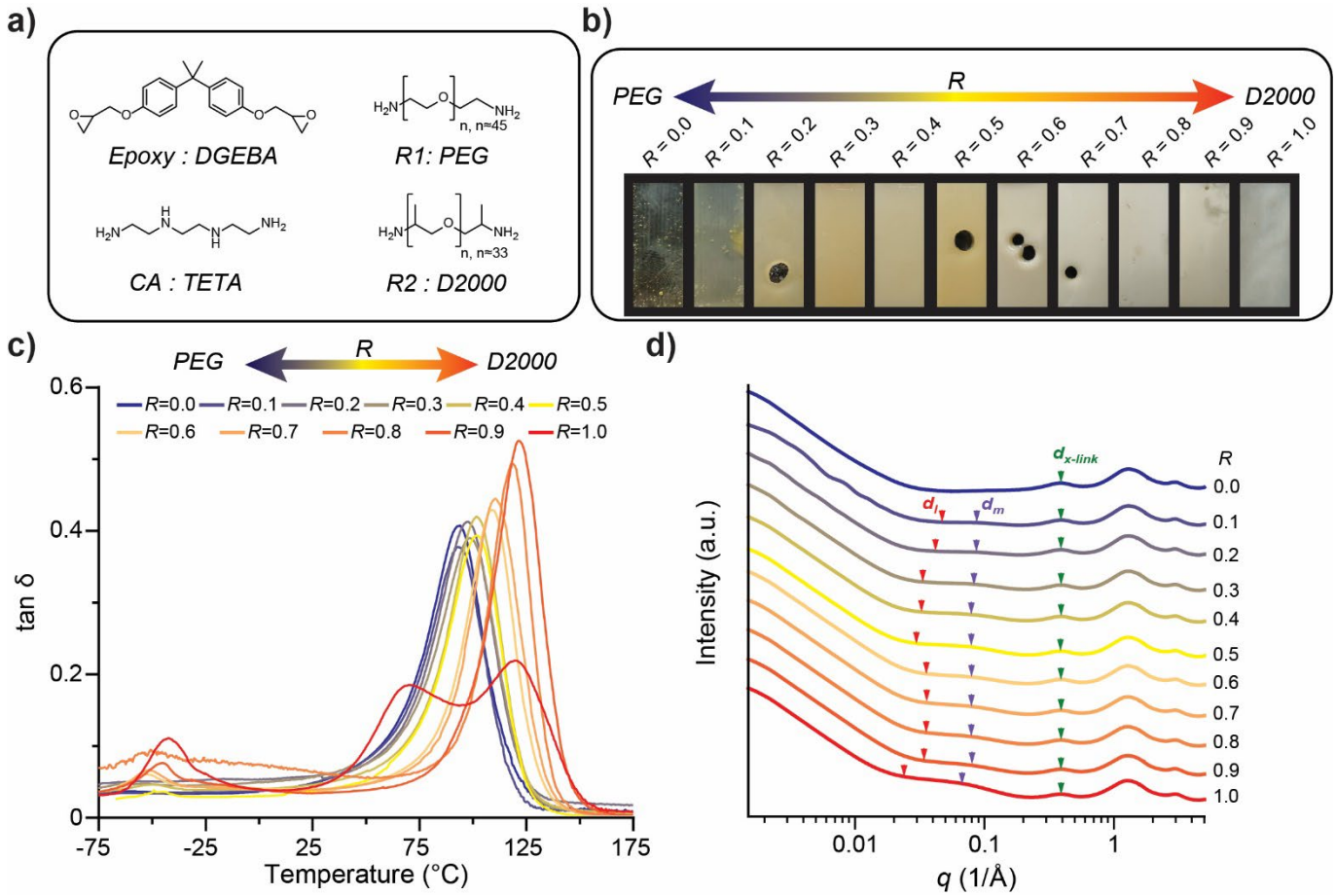

Figure 5. Tunable PIPS by exploiting a binary rubber mixture. (a) Chemical structures of DGEBA, D2000, PEG, and TETA. (b) Images of plaques, (c) loss tangent vs. temperature, and (d) SWAXS patterns for rubber-tuned epoxies with m=0.1 and varied R.

largest. Importantly, the peak in loss tangent at e=0 is both narrow and tall, consistent with the very shallow q_m feature in the corresponding X-ray scattering data, suggesting weak nanophase separation or complete miscibility at the molecular level – a phenomenon not seen in the CA-tuned system.

Finally, to investigate tuning of PIPS using a binary rubber, we compared diamine-functionalized poly(propylene glycol) (D2000) to diamine-functionalized poly(ethylene glycol) (PEG) of similar chain length, with DGEBA and TETA as the epoxy resin and CA, respectively. D2000 was found to have poor miscibility with TETA-crosslinked DGEBA, whereas PEG is known to be highly miscible with DGEBA-based epoxies.[57] As anticipated, plaques made purely with PEG as rubber formed transparent plaques, whereas those made purely with D2000 formed opaque plaques (Figure 5). Thus, a binary mixture was created with the purpose of fine-tuning morphology, where R denotes the ratio of PEG to D2000, where R=0.0 and R=1.0 correspond to entirely PEG and entirely D2000, respectively. The rubber-tuned materials showed a greater propensity towards macrophase separation: with a total rubber content of m=0.1, only R=0.0 produces a transparent material with R=0.1 yielding the blue tint associated with metastability and larger values of R producing opaque, macrophase separated samples.

Unlike the CA- or resin-tuned epoxies, the rubber-tuned materials show little variation in the key scattering features (Figure 5d and Table S6). The crosslink length $d_{x\text{-link}}$ was expected to be relatively invariant, as the composition of the CA and epoxide are constant in this case. On the other hand, we were surprised to find that the nanoscale domains, as defined by d_l and d_m, are also relatively invariant, despite the existence of transparent, cloudy, and opaque samples across this series of materials. The relatively suppressed and invariant d_l and d_m indicate that the compositional fluctuation along m=0.1 is relatively weak. Gratifyingly, however, the scattering trends are consistent with the glass transitions, as little variation in the breadth of T_g occurs as the rubber composition is tuned. R = 1 is an outlier, but we note that this system has the widest macrophase separated window of any system investigated. We speculate that the phase separation may be so extreme at R = 1 as to inhibit complete reaction of functional groups, leading to the formation of additional phases with different local crosslink densities along with a concomitant, complex glass transition profile. It is important to note that the reaction rates of the rubbers are slower compared to the CAs, thus the probability of both PEG and D2000 being found in the same molecule during phase separation is low. At any R > 0, macrophase separation of D2000 from DGEBA-TETA dominates as the outcome of PIPS, with PEG miscible in the epoxy or rubber domains, or perhaps both. In contrast, with CA- or resin-tuning, the probability of D230/TETA or DGEBA/DER being found in the same molecule during phase separation is higher, thus the phase behaviour is

governed by the relative compositions of those chain segments. In both cases the coupling between nanoscale structure and the dynamic heterogeneity of these materials, modulated by the macrophase separation behaviour, is uniquely illustrated through the tuneable nature of the formulations.

Conclusions

Using simple and fast X-ray scattering measurements, we have found that PIPS in reactive mixtures consisting of epoxy resin, amine curing agent (CA), and rubber proceeds initially through compositional fluctuations which cause nanoscale and/or macroscale phase separation of epoxy and rubber components prior to additional local chain crosslinking. The finer details of the phase-separated structure are controlled by the reactivities of the constituents and the interactions of the chain segments formed. We have shown that morphology can be tuned by modulating these characteristics efficiently via the composition of the constituents. We have illustrated this tuneability using both CA tuning, resin tuning, and rubber tuning. It was found that CA and resin tuning yield greater diversity in the range of achievable nanoscale features. The glass transition is intimately coupled to the nanoscale and macroscale structures, thus CA and resin tuning also gave a broader range of glass transitions in terms of position, breadth, and single or multiple relaxations. We anticipate that the phase behaviour established in these systems can be similarly utilized or further extended to develop crosslinked step-growth polymers with precisely optimized properties.

Author Contributions

The manuscript was written through contributions of all authors. All authors have given approval to the final version of the manuscript. **Samuel C. Leguizamon**: Conceptualization, Methodology, Validation, Investigation, Data curation, Writing - original draft, Writing - review & editing. **Juhong Ahn**: Conceptualization, Methodology, Validation, Investigation, Data curation, Writing - original draft, Writing - review & editing. **Sangwoo Lee**: Conceptualization, Methodology, Validation, Resources, Writing - original draft, Writing - review & editing, Visualization, Supervision. **Brad H. Jones**: Conceptualization, Methodology, Validation, Investigation, Resources, Data curation, Writing - original draft, Writing - review & editing, Visualization, Supervision, Project administration, Funding acquisition.

Conflicts of interest

There are no conflicts to declare

Acknowledgements

We thank Leah Appelhans and Jim McElhanon for their review of the manuscript. Any subjective views or opinions that might be expressed in the paper do not necessarily represent the views of the U.S. Department of Energy (DOE) or the U.S. Government. Sandia National Laboratories is a multi-mission laboratory managed and operated by National Technology and Engineering Solutions of Sandia, LLC, a wholly owned subsidiary of Honeywell International, Inc., for the U.S. Department of Energy's National Nuclear Security Administration under contract DE-NA-0003525. This research used resources of the 12-ID beamline of the National Synchrotron Light Source II, a U.S. Department of Energy (DOE) Office of Science User Facility operated for the DOE Office of Science by Brookhaven National Laboratory under Contract No. DESC0012704; and the 9-ID-C of the Advanced Photon Source, a U.S. Department of Energy (DOE) Office of Science User Facility, operated for the DOE Office of Science by Argonne National Laboratory under Contract No. DE-AC02-06CH11357.

References

1. M. A. Hillmyer, P. M. Lipic, D. A. Hajduk, K. Almdal and F. S. Bates, *J. Am. Chem. Soc.*, 1997, **119**, 2749-2750.
2. P. M. Lipic, F. S. Bates and M. A. Hillmyer, *J. Am. Chem. Soc.*, 1998, **120**, 8963-8970.
3. H. Garate, N. J. Morales, S. Goyanes and N. B. D'Accorso, in *Handbook of Epoxy Blends*, eds. J. Parameswaranpillai, N. Hameed, J. Pionteck and E. M. Woo, Springer International Publishing, Cham, 2017, DOI: 10.1007/978-3-319-40043-3_31, pp. 841-881.
4. M. W. Schulze and M. A. Hillmyer, *Macromolecules*, 2017, **50**, 997-1007.
5. Y. Meng and X. Zhang, Nanostructured Epoxy Composites. In *Micro- and Nanostructured Epoxy/Rubber Blends* (eds S. Thomas, C. Sinturel and R. Thomas), 2014
6. S. Dubinsky, A. Petukhova, I. Gourevich and E. Kumacheva, *Chem. Commun.*, 2010, **46**, 2578-2580.
7. J. Park, S. A. Saba, M. A. Hillmyer, D.-C. Kang and M. Seo, *Polymer*, 2017, **126**, 338-351.
8. A. A. Gavrilov and A. V. Chertovich, *Polymers*, 2020, **12**, 2637.
9. S. A. Saba, B. Lee and M. A. Hillmyer, *ACS Macro Lett.*, 2017, **6**, 1232-1236.
10. C. E. Hoppe, M. J. Galante, P. A. Oyanguren and R. J. J. Williams, *Macromolecules*, 2002, **35**, 6324-6331.
11. M. Okada, K. Fujimoto and T. Nose, *Macromolecules*, 1995, **28**, 1795-1800.
12. R. Yu, S. Zheng, X. Li and J. Wang, *Macromolecules*, 2012, **45**, 9155-9168.
13. J. Oh and A. D. Rey, *Comput. Theor. Polym. Sci.*, 2001, **11**, 205-217.
14. E. S. Zofchak, J. A. LaNasa, V. M. Torres and R. J. Hickey, *Macromolecules*, 2020, **53**, 835-843.
15. Y. Tang, K. Wu, S. Yu, J. Chen, X. Ding, L. Rao and Z. Li, *Opt. Lett.*, 2020, **45**, 2918-2921.
16. D. C. Hoekstra, B. P. A. C. van der Lubbe, T. Bus, L. Yang, N. Grossiord, M. G. Debije and A. P. H. J. Schenning, *Angew. Chem. Int. Ed.*, DOI: 10.1002/anie.202101322.
17. V. Rebizant, A.-S. Venet, F. Tournilhac, E. Girard-Reydet, C. Navarro, J.-P. Pascault and L. Leibler, *Macromolecules*, 2004, **37**, 8017-8027.
18. B. J. P. Jansen, S. Rastogi, H. E. H. Meijer and P. J. Lemstra, *Macromolecules*, 2001, **34**, 3998-4006.

19. J. Wang, X. Zhang, L. Jiang and J. Qiao, *Prog. Polym. Sci.*, 2019, **98**, 101160.
20. W. Chonkaew and N. Sombatsompop, *J. Appl. Polym. Sci.*, 2012, **125**, 361-369.
21. Z. Heng, X. Zhang, Y. Chen, H. Zou and M. Liang, *Chem. Eng. J.*, 2019, **360**, 542-552.
22. L.-Z. Guan, L.-X. Gong, L.-C. Tang, L.-B. Wu, J.-X. Jiang and G.-Q. Lai, *Polym. Compos.*, 2015, **36**, 785-799.
23. S.-A. Xu and X.-X. Song, in *Handbook of Epoxy Blends*, eds. J. Parameswaranpillai, N. Hameed, J. Pionteck and E. M. Woo, Springer International Publishing, Cham, 2015, DOI: 10.1007/978-3-319-18158-5_1-1, pp. 1-26.
24. Z. Dong, H. Cui, H. Zhang, F. Wang, X. Zhan, F. Mayer, B. Nestler, M. Wegener and P. A. Levkin, *Natur. Commun.*, 2021, **12**, 247.
25. A. G. Loera, F. Cara, M. Dumon and J. P. Pascault, *Macromolecules*, 2002, **35**, 6291-6297.
26. S. A. Chopade, J. G. Au, Z. Li, P. W. Schmidt, M. A. Hillmyer and T. P. Lodge, *ACS Appl. Mater. Interf.*, 2017, **9**, 14561-14565.
27. M. W. Schulze, L. D. McIntosh, M. A. Hillmyer and T. P. Lodge, *Nano Lett.*, 2014, **14**, 122-126.
28. L. M. Schneider, N. Ihrner, D. Zenkert and M. Johansson, *ACS Appl. Ener. Mater.*, 2019, **2**, 4362-4369.
29. A. Sicher, R. Ganz, A. Menzel, D. Messmer, G. Panzarasa, M. Feofilova, R. O. Prum, R. W. Style, V. Saranathan, R. M. Rossi and E. R. Dufresne, *Soft Matter*, 2021, **17**, 5772-5779.
30. N. Kumano, T. Seki, M. Ishii, H. Nakamura and Y. Takeoka, *Angew. Chem. Int. Ed.*, 2011, **50**, 4012-4015.
31. Q.-H. Le, H.-C. Kuan, J.-B. Dai, I. Zaman, L. Luong and J. Ma, *Polymer*, 2010, **51**, 4867-4879.
32. L.-C. Tang, X. Wang, Y.-J. Wan, L.-B. Wu, J.-X. Jiang and G.-Q. Lai, *Mater. Chem. Phys.*, 2013, **141**, 333-342.
33. C. B. Bucknall and D. R. Paul, *Polymer*, 2013, **54**, 320-329.
34. K. A. Masser, E. D. Bain, F. L. Beyer, A. M. Savage, J. H. Yu and J. L. Lenhart, *Polymer*, 2016, **103**, 337-346.
35. Q. Meng, S. Araby, N. Saber, H.-C. Kuan, J. Dai, L. Luong, J. Ma and C. H. Wang, *J. Mater. Res.*, 2014, **29**, 665-674.
36. R. Motokawa, Y. Iida, Y. Zhao, T. Hashimoto and S. Koizumi, *Polym. J.*, 2007, **39**, 1312-1318.
37. E. S. Zofchak, J. A. LaNasa, W. Mei and R. J. Hickey, *ACS Macro Lett.*, 2018, **7**, 822-827.
38. L. Li, W. Peng, L. Liu and S. Zheng, *Polym. Eng. Sci.*, 2022, **62**, 392-404.
39. S. C. Leguizamon, J. Powers, J. Ahn, S. Dickens, S. L. Lee and B. H. Jones, *Macromolecules*, 2021, **54**, 7796–7807.
40. V.-N. Tran Duc and P. K. Chan, *ChemEngineering*, 2019, **3**, 75.
41. R. Alert, P. Tierno and J. Casademunt, *Nat. Commun.*, 2016, **7**, 13067.
42. K. Kim, M. W. Schulze, A. Arora, R. M. Lewis, M. A. Hillmyer, K. D. Dorfman and F. S. Bates, *Science*, 2017, **356**, 520-523.
43. P. J. Flory, *J. Chem. Phys.*, 1942, **10**, 51-61.
44. P. J. Flory, *Principles of polymer chemistry*, Cornell University Press, Ithaca, New York, 1953.
45. M. L. Huggins, *J. Am. Chem. Soc*, 1942, **64**, 1712-1719.
46. M. L. Huggins, *J. Phys. Chem*, 1942, **46**, 151-158.
47. C. Ayyagari, D. Bedrov and G. D. Smith, *Macromolecules*, 2000, **33**, 6194-6199.
48. C. Herkt-Maetzky and J. Schelten, *Phys. Rev. Lett.*, 1983, **51**, 896-899.
49. F. S. Bates and P. Wiltzius, *J. Phys. Chem*, 1989, **91**, 3258-3274.
50. J. Cabral and J. Higgins, *Prog. Polym. Sci.*, 2018, **81**, 1-21.
51. N. Takano, Y. Einaga and H. Fujita, *Polym. J.*, 1985, **17**, 1123-1130.
52. B. H. Jones, T. M. Alam, S. Lee, M. C. Celina, J. P. Allers, S. Park, L. Chen, E. J. Martinez and J. L. Unangst, *Polymer*, 2020, **205**, 122783.
53. K. A. Masser, D. B. Knorr, M. D. Hindenlang, J. H. Yu, A. D. Richardson, K. E. Strawhecker, F. L. Beyer and J. L. Lenhart, *Polymer*, 2015, **58**, 96-106.
54. K. A. Masser, D. B. Knorr Jr., J. H. Yu, M. D. Hindenlang and J. L. Lenhart, *J. Appl. Polym. Sci.*, 2016, **133**.
55. J. Huang, Y. Xu, S. Qi, J. Zhou, W. Shi, T. Zhao and M. Liu, *Nat. Commun.*, 2021, **12**, 3610.
56. S. Ye, N. B. Cramer and C. N. Bowman, *Macromolecules*, 2011, **44**, 490-494.
57. X. Luo, S. Zheng, N. Zhang and D. Ma, *Polymer*, 1994, **35**, 2619-2623.

Supplementary Information for

Tuneable Phase Behaviour and Glass Transition via Polymerization-Induced Phase Separation in Crosslinked Step-Growth Polymers

Samuel C. Leguizamon[a]; Juhong Ahn[b]; Sangwoo Lee[b]; Brad H. Jones[a,*]

[a] Department of Organic Materials Science, Sandia National Laboratories, Albuquerque, NM, 87185, USA

[b] Department of Chemical and Biological Engineering, Rensselaer Polytechnic Institute, Troy, NY, 12180, USA

Experimental Section:

Materials and Sample Preparation. Triethylenetetramine (TETA) and poly(ethylene glycol) diamine (PEG, M_w 2000) were obtained from Millipore Sigma (Burlington, MA USA). Jeffamines D230, D2000, and T3000 were obtained from Huntsman Corporation. EPON 828, a diglycidyl ether of bisphenol A (DGEBA), was obtained from Miller-Stephenson (Sylmar, CA USA). D.E.R. 732 (DER) was obtained from Palmer Holland (North Olmsted, OH USA). All reagents were used as received.

Mixtures of DGEBA and curing agents bearing epoxy or amine functional groups, respectively, were prepared so that epoxies and amine hydrogens were kept at a constant stoichiometric ratio (*i.e.*, $r = [-NH-]_{0,total}/[epoxide]_{0,total} = 1$), while the fraction of amine hydrogens from T3000 was varied and defined by the value $m = [-NH-]_{0,T3000}/[-NH-]_{0,total}$, where $[-NH-]_{0,T3000}$ and $[-NH-]_{0,total}$ are the initial molar concentrations of T3000 amine hydrogens and total amine hydrogens in the mixture, respectively. The remaining amine hydrogens were provided by curing agents with concentrations described by $n = [-NH-]_{0,TETA}/([-NH-]_{0,D230} + [-NH-]_{0,TETA})$, where $[-NH-]_{0,D230}$ and $[-NH-]_{0,TETA}$ are the initial molar concentrations of amine hydrogens from the binary curing agent mixture. Similarly, mixtures incorporating DER 732, PEG, and/or D2000 were kept at a constant stoichiometric ratio (*i.e.*, $r = [-NH-]_{0,total}/[epoxide]_{0,total} = 1$), while the fraction of amine hydrogens from rubbers was varied to account for a mole fraction of 0.1 in total. In the DER-DGEBA-T3000-TETA system, the total epoxy functional groups was kept constant but attributing epoxy-bearing species were varied by $e = [epoxide]_{0,DER732}/([epoxide]_{0,DGEBA} + [epoxide]_{0,DER732})$, where $[epoxide]_{0,DGEBA}$ and $[epoxide]_{0,DER732}$ are the initial molar concentrations of epoxides from the binary epoxide mixture. In the DGEBA-PEG-D2000-TETA system, the amine hydrogens from rubbers were described by $R = [-NH-]_{0,D2000}/([-NH-]_{0,PEG} +$

$[-NH-]_{0,D2000}$), where $[-NH-]_{0,PEG}$ and $[-NH-]_{0,D2000}$ are the initial molar concentrations of amine hydrogens from the binary rubber mixture

Desired amounts of amine bearing species defined by *n*, *m,* and/or *R* were mixed in a Thinky planetary centrifugal mixer prior to addition of DGEBA and/or DER 732 and a second round of centrifugal mixing. The homogeneous, uncured liquid was then spread into a silicone mold to obtain the desired shape for mechanical testing (i.e., rectangular plaques). The cure temperature was controlled by placing the silicone mold in a temperature-controlled oven, yielding thin, solid, rectangular plaques that were easily demolded from the mold cavity. Previous work showed there is no dependence on final morphology or thermomechanical properties on cure temperature below 140°C,[1] therefore samples in this study were cured isothermally at 100°C for 24h and compared with the previous samples cured at 60°C.

Formulations are shown in Table S1.

Dynamic Mechanical Analysis (DMA). DMA was performed using a strain-controlled Rheometric Scientific (Piscataway, NJ, USA) ARES-LS/M rheometer operating in small-amplitude oscillatory shear. The dynamic shear storage (G') and loss (G'') moduli and loss tangent (G''/G') of the thin rectangular plaques described above were measured using torsional deformation with 1 Hz oscillation frequency, 0.5% strain amplitude, and a ramp rate of 3°C/min. Measurements were conducted upon heating from 25°C to 200°C, followed by subsequent cooling from 200°C to -75°C. The samples were assumed to be fully cured after heating to 200°C, thus data are presented from the cooling cycle unless otherwise noted.

X-ray Scattering. Small- and wide-angle X-ray scattering (SWAXS) characterization of the thermosets was conducted at the 12-ID beamline at the National Synchrotron Light Source-II

(NSLS-II), Brookhaven National Laboratory, NY. Two-dimensional (2D) scattering patterns were recorded using Pilatus 1M and 300kW and 300kW detectors (Dectris, Switzerland) located at 8,300 mm and 275 mm away from the sample, respectively. The reciprocal space over the scattering vector $q = 4\pi \cdot \sin(\theta/2)/\lambda$ from 0.003 $Å^{-1}$ to 5 $Å^{-1}$ where the θ is the scattering angle and $\lambda = 0.8920$ Å was interrogated for the structure analysis. All sample measurements were conducted under vacuum (< 10^{-3} Torr) at 25 °C unless noted otherwise.

The time resolved X-ray scattering characterization over the DGEBA-T3000-D230-TETA sample under curing was conducted using the HFSX350 capillary stage (Linkam). The precursor solutions of the samples were prepared at 25 °C by mixing DGEBA and curing agents, the mixtures were immediately loaded in quartz capillaries of the nominal diameter of 1.5 mm (Charles-Supper), sealed using bee waxes (Hampton Research), and the time-resolved X-ray-scattering measurements were conducted at elevated temperatures.

Table S1. Formulations investigated in this work defined by *n*, *m*, *e*, and *R* with wt% of each reagent shown.

m	*n*	DGEBA wt%	T3000 wt%	TETA wt %	D230 wt %
0.025	0	73.3	4.9	0.0	21.8
0.025	0.1	74.3	4.9	0.9	19.9
0.025	0.2	75.2	5.0	1.9	17.9
0.025	0.3	76.2	5.1	2.9	15.9
0.025	0.4	77.2	5.1	3.9	13.8
0.025	0.5	78.2	5.2	4.9	11.6
0.025	0.6	79.3	5.3	6.0	9.4
0.025	0.7	80.4	5.3	7.1	7.2
0.025	0.8	81.5	5.4	8.2	4.8
0.025	0.9	82.7	5.5	9.4	2.5
0.025	1	83.9	5.6	10.6	0.0
0.1	0	64.9	17.2	0.0	17.8
0.1	0.1	65.6	17.4	0.8	16.2
0.1	0.2	66.3	17.6	1.5	14.6
0.1	0.3	67.0	17.8	2.3	12.9
0.1	0.4	67.7	18.0	3.2	11.2
0.1	0.5	68.5	18.2	4.0	9.4
0.1	0.6	69.2	18.4	4.8	7.6
0.1	0.7	70.0	18.6	5.7	5.8
0.1	0.8	70.8	18.8	6.6	3.9
0.1	0.9	71.6	19.0	7.5	2.0
0.1	1	72.4	19.2	8.4	0.0

m	*n*	DGEBA wt%	T3000 wt%	TETA wt %	D230 wt %
0.2	0	56.4	29.9	0.0	13.8
0.2	0.1	56.8	30.1	0.6	12.5
0.2	0.2	57.3	30.4	1.2	11.2
0.2	0.3	57.7	30.6	1.8	9.9
0.2	0.4	58.2	30.9	2.4	8.5
0.2	0.5	58.7	31.1	3.0	7.2
0.2	0.6	59.2	31.4	3.7	5.8
0.2	0.7	59.7	31.7	4.3	4.4
0.2	0.8	60.2	31.9	5.0	2.9
0.2	0.9	60.7	32.2	5.6	1.5
0.2	1	61.2	32.5	6.3	0.0
0.3	0	49.8	39.6	0.0	10.6
0.3	0.1	50.1	39.8	0.5	9.6
0.3	0.2	50.4	40.1	0.9	8.6
0.3	0.3	50.7	40.3	1.4	7.6
0.3	0.4	51.0	40.6	1.8	6.5
0.3	0.5	51.3	40.9	2.3	5.5
0.3	0.6	51.7	41.1	2.8	4.4
0.3	0.7	52.0	41.4	3.3	3.3
0.3	0.8	52.3	41.6	3.8	2.2
0.3	0.9	52.7	41.9	4.3	1.1
0.3	1	53.0	42.2	4.8	0.0

m	*n*	DGEBA wt%	T3000 wt%	TETA wt %	D230 wt %
0.4	0	44.6	47.3	0.0	8.2
0.4	0.1	44.8	47.5	0.3	7.4
0.4	0.2	45.0	47.7	0.7	6.6
0.4	0.3	45.2	48.0	1.1	5.8
0.4	0.4	45.4	48.2	1.4	5.0
0.4	0.5	45.6	48.4	1.8	4.2
0.4	0.6	45.9	48.7	2.1	3.4
0.4	0.7	46.1	48.9	2.5	2.5
0.4	0.8	46.3	49.1	2.9	1.7
0.4	0.9	46.5	49.4	3.2	0.9
0.4	1	46.8	49.6	3.6	0.0
0.5	0	40.3	53.5	0.0	6.2
0.5	0.1	40.5	53.7	0.3	5.6
0.5	0.2	40.6	53.9	0.5	5.0
0.5	0.3	40.8	54.1	0.8	4.4
0.5	0.4	40.9	54.3	1.1	3.7
0.5	0.5	41.1	54.5	1.3	3.1
0.5	0.6	41.2	54.7	1.6	2.5
0.5	0.7	41.4	54.9	1.9	1.9
0.5	0.8	41.5	55.1	2.1	1.3
0.5	0.9	41.7	55.3	2.4	0.6
0.5	1	41.8	55.5	2.7	0.0

m	*n*	DGEBA wt%	T3000 wt%	TETA wt %	D230 wt %
0.6	0.0	36.9	58.7	0.0	4.5
0.6	0.1	36.9	58.8	0.2	4.1
0.6	0.2	37.0	59.0	0.4	3.6
0.6	0.3	37.1	59.1	0.6	3.2
0.6	0.4	37.2	59.3	0.8	2.7
0.6	0.5	37.3	59.4	1.0	2.3
0.6	0.6	37.4	59.6	1.2	1.8
0.6	0.7	37.5	59.7	1.4	1.4
0.6	0.8	37.6	59.9	1.6	0.9
0.6	0.9	37.7	60.1	1.8	0.5
0.6	1.0	37.8	60.2	2.0	0.0
0.7	0.0	33.9	63.0	0.0	3.1
0.7	0.1	34.0	63.1	0.1	2.8
0.7	0.2	34.0	63.2	0.3	2.5
0.7	0.3	34.1	63.3	0.4	2.2
0.7	0.4	34.2	63.4	0.5	1.9
0.7	0.5	34.2	63.5	0.7	1.6
0.7	0.6	34.3	63.7	0.8	1.3
0.7	0.7	34.3	63.8	0.9	0.9
0.7	0.8	34.4	63.9	1.1	0.6
0.7	0.9	34.5	64.0	1.2	0.3
0.7	1.0	34.5	64.1	1.3	0.0

m	*n*	DGEBA wt%	T3000 wt%	TETA wt %	D230 wt %
0.8	0	31.4	66.7	0.0	1.9
0.8	0.1	31.5	66.7	0.1	1.7
0.8	0.2	31.5	66.8	0.2	1.5
0.8	0.3	31.5	66.9	0.2	1.3
0.8	0.4	31.6	67.0	0.3	1.2
0.8	0.5	31.6	67.0	0.4	1.0
0.8	0.6	31.6	67.1	0.5	0.8
0.8	0.7	31.7	67.2	0.6	0.6
0.8	0.8	31.7	67.3	0.7	0.4
0.8	0.9	31.7	67.3	0.7	0.2
0.8	1	31.8	67.4	0.8	0.0
0.9	0	29.3	69.8	0.0	0.9
0.9	0.1	29.3	69.9	0.0	0.8
0.9	0.2	29.3	69.9	0.1	0.7
0.9	0.3	29.3	70.0	0.1	0.6
0.9	0.4	29.3	70.0	0.2	0.5
0.9	0.5	29.3	70.0	0.2	0.4
0.9	0.6	29.3	70.1	0.2	0.4
0.9	0.7	29.4	70.1	0.3	0.3
0.9	0.8	29.4	70.1	0.3	0.2
0.9	0.9	29.4	70.2	0.3	0.1
0.9	1	29.4	70.2	0.4	0.0

m	*e*	DGEBA wt%	DER 732 wt%	T3000 wt%	TETA wt %
0.1	0	0.0	81.6	12.8	5.6
0.1	0.1	5.0	76.0	13.2	5.8
0.1	0.2	10.3	70.0	13.7	6.0
0.1	0.3	16.0	63.5	14.2	6.2
0.1	0.4	22.2	56.6	14.7	6.5
0.1	0.5	28.9	49.1	15.3	6.7
0.1	0.6	36.1	40.9	16.0	7.0
0.1	0.7	44.0	32.0	16.7	7.3
0.1	0.8	52.6	22.3	17.4	7.6
0.1	0.9	62.0	11.7	18.3	8.0
0.1	1	72.4	0.0	19.2	8.4

m	*R*	DGEBA wt%	PEG wt%	D2000 wt %	TETA wt %
0.1	0	72.4	19.2	0.0	8.4
0.1	0.1	72.4	17.3	1.9	8.4
0.1	0.2	72.4	15.4	3.8	8.4
0.1	0.3	72.4	13.4	5.8	8.4
0.1	0.4	72.4	11.5	7.7	8.4
0.1	0.5	72.4	9.6	9.6	8.4
0.1	0.6	72.4	7.7	11.5	8.4
0.1	0.7	72.4	5.8	13.4	8.4
0.1	0.8	72.4	3.8	15.4	8.4
0.1	0.9	72.4	1.9	17.3	8.4
0.1	1	72.4	0.0	19.2	8.4

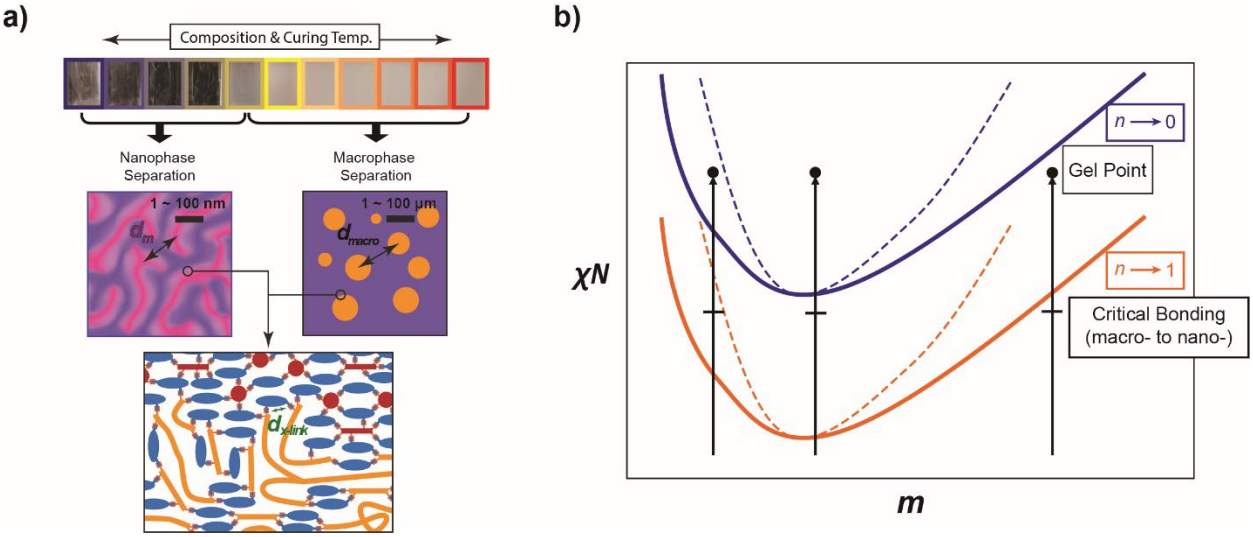

Figure S1. Schematic illustrations of phase separation process in CA-tuned epoxies. (a) Nanophase separation and macrophase separation into domains defined by characteristic length scales d_m and d_{macro}, respectively. The expanded area shows a cartoon representation of the domain interfaces with blue ovals, red circles/lines, and yellow lines indicating the epoxy, binary CA, and rubber components of the network, respectively. $d_{x\text{-}link}$ is the characteristic length scale of the highly crosslinked domains. (b) A generalized representation of the impact of mixture composition on the curing and phase separation in the context of classic Flory-Huggins phase space. χN is the product of the Flory-Huggins interaction parameter and the degree of polymerization of the network, *i.e.*, the extent of epoxide conversion. The solid blue and orange lines indicate a binodal curve for smaller and larger n, respectively, while the dotted blue and orange lines indicate the corresponding spinodal curves. At smaller n, the epoxy-CA network is more compatible with the rubber (mean χ decreases in the pseudo-binary phase diagram of χN and m of the panel b), thus a larger N is needed to cross the phase boundary. At larger n, the epoxy-CA network is less compatible with the rubber (mean χ increases), thus a smaller N is needed to cross the phase boundary. Each arrow represents the cure of a mixture with different rubber content m, starting at $N = 1$ and curing through the gel (or vitrification) point, at which phase separation is arrested. The hash mark indicates a hypothetical point at which enough bonds have formed between epoxy and rubber to favor nanoscale over macroscale morphologies. The position of this hash mark should depend on the relative reactivities of the various amine constituents, with a faster reacting rubber shifting the hash mark lower on the arrow. This generalized representation would be the same for resin- and rubber-tuned materials, with n being replaced by e or R, respectively.

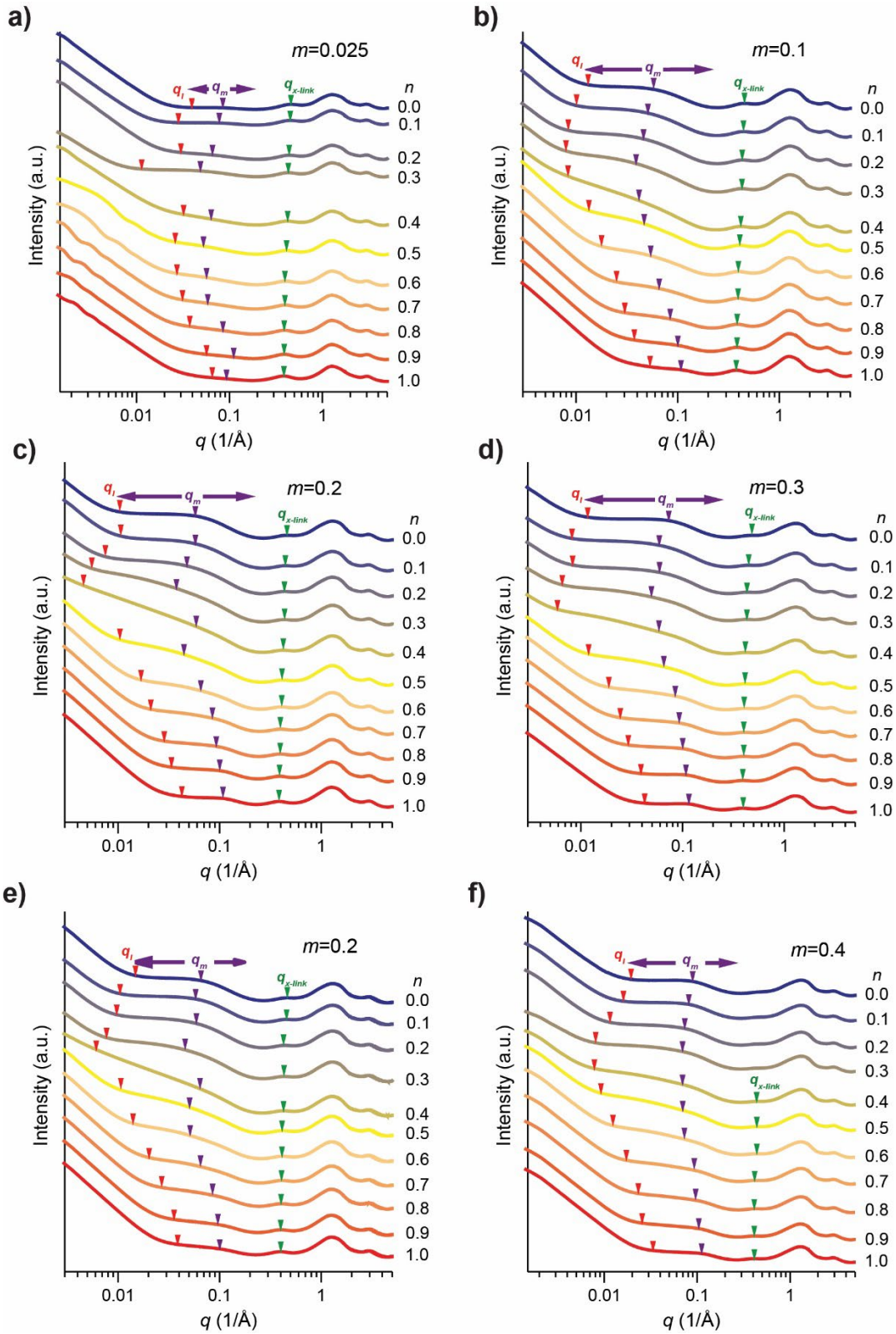
a)
m=0.025
b)
m=0.1
c)
m=0.2
d)
m=0.3
e)
m=0.2
f)
m=0.4
q_l
q_m
q_x-link
n
0.0
0.1
0.2
0.3
0.4
0.5
0.6
0.7
0.8
0.9
1.0
Intensity (a.u.)
q (1/Å)
0.01
0.1
1

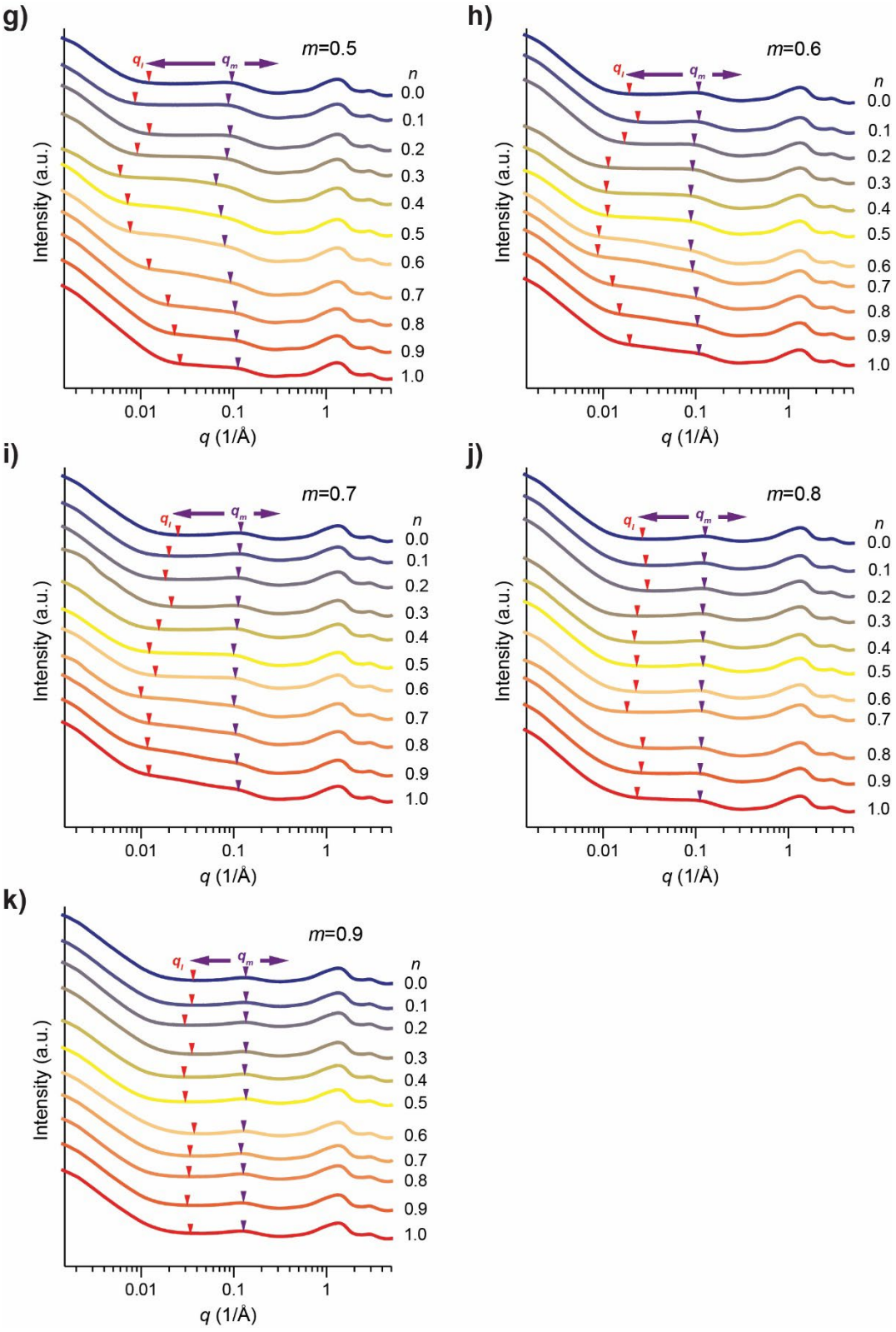

Figure S2. X-ray scattering of fully cured CA-tuned epoxies. SWAXS patterns of samples cured at (a-d) 60°C and (e-k) 100°C.

Table S2. The longest wavelength of compositional fluctuation, d_l, of the ETTD systems with m = 0.025 - 0.3 cured at 60 °C and m =0.2 - 0.9 cured at 100 °C.

n	m										
	d_l (nm) of ETTD cured at 60 °C				d_l (nm) of ETTD cured at 100 °C						
	0.025	**0.1**	**0.2**	**0.3**	**0.2**	**0.4**	**0.5**	**0.6**	**0.7**	**0.8**	**0.9**
0.0	16.7	48.0	63.6	53.1	41.2	32.3	48.1	32.7	26.6	22.3	16.9
0.1	22.8	59.1	59.1	78.1	59.2	41.8	64.3	26.9	32.0	21.9	18.1
0.2	21.3	77.1	85.1	74.6	63.5	52.5	49.8	37.4	35.5	21.3	21.1
0.3	54.2	75.7	117.1	93.1	79.3	78.3	65.8	56.7	30.0	31.6	18.2
0.4	16.8	75.2	149.8	107.5	66.1	82.9	104.0	53.5	42.4	27.9	21.3
0.5	23.5	48.3	61.4	51.7	56.5	67.3	88.0	54.5	51.5	26.6	22.4
0.6	22.7	35.7	37.4	33.7	46.1	48.9	78.3	72.4	45.0	29.0	16.1
0.7	18.4	24.8	30.8	26.2	31.2	36.9	52.5	70.6	65.8	39.5	19.7
0.8	15.7	22.0	22.1	21.6	23.9	28.2	32.7	49.8	51.5	24.8	23.4
0.9	10.4	16.0	18.7	16.8	18.5	25.2	27.4	42.4	57.8	26.1	19.9
1.0	9.0	12.0	15.1	14.8	16.7	19.0	24.3	33.5	51.5	27.6	18.2

Table S3. The wavelength of compositional fluctuation, d_m, of the ETTD systems with m = 0.025 - 0.3 cured at 60 °C and m =0.2 - 0.9 cured at 100 °C.

n	m										
	d_m (nm) of ETTD cured at 60 °C				d_m (nm) of ETTD cured at 100 °C						
	0.025	**0.1**	**0.2**	**0.3**	**0.2**	**0.4**	**0.5**	**0.6**	**0.7**	**0.8**	**0.9**
0.0	7.4	10.8	10.9	8.6	9.6	7.1	6.5	5.8	5.3	4.9	4.7
0.1	8.1	12.3	10.8	10.6	10.8	7.7	7.1	5.8	5.4	5.1	4.7
0.2	9.6	13.6	13.2	10.7	10.7	8.6	6.8	6.5	5.6	5.1	4.7
0.3	12.9	16.1	16.7	12.7	13.7	9.0	7.4	6.8	5.6	5.3	4.7
0.4	15.6	15.1	10.7	10.7	9.8	9.0	9.7	7.1	5.8	5.3	4.8
0.5	18.8	13.4	14.0	9.6	12.4	9.0	8.6	7.1	6.3	5.3	4.7
0.6	17.4	11.6	9.6	7.4	12.3	8.6	7.7	7.1	6.0	5.4	4.9
0.7	16.9	9.6	7.4	6.8	9.7	6.8	6.8	6.8	6.3	5.4	5.3
0.8	11.8	7.4	6.8	6.3	7.4	6.5	6.0	6.3	6.0	5.4	4.9
0.9	8.9	6.3	6.3	5.8	6.5	6.0	5.8	6.0	5.8	5.6	4.9
1.0	10.8	5.8	5.8	5.4	6.3	5.6	5.6	5.8	5.6	5.6	4.9

Table S4. The wavelength of crosslink, $d_{x\text{-}link}$, of the ETTD systems with m = 0.025 - 0.3 cured at 60 °C and m =0.2 - 0.9 cured at 100 °C.

n	m										
	$d_{x\text{-}link}$ (nm) of ETTD cured at 60 °C				$d_{x\text{-}link}$ (nm) of ETTD cured at 100 °C						
	0.025	**0.1**	**0.2**	**0.3**	**0.2**	**0.4**	**0.5**	**0.6**	**0.7**	**0.8**	**0.9**
0.0	1.4	1.38	1.36	-	1.4	-	-	-	-	-	-
0.1	1.4	1.41	1.42	1.4	1.4	-	-	-	-	-	-
0.2	1.4	1.44	1.44	1.5	1.4	-	-	-	-	-	-
0.3	1.5	1.46	1.46	1.5	1.5	-	-	-	-	-	-
0.4	1.5	1.5	1.48	1.5	1.5	1.4	-	-	-	-	-
0.5	1.5	1.54	1.53	1.5	1.5	1.4	-	-	-	-	-
0.6	1.6	1.55	1.54	1.5	1.5	1.4	-	-	-	-	-
0.7	1.6	1.6	1.58	1.6	1.5	1.5	-	-	-	-	-
0.8	1.6	1.63	1.58	1.6	1.6	1.5	-	-	-	-	-
0.9	1.62	1.63	1.62	1.6	1.57	1.53	-	-	-	-	-
1.0	1.63	1.67	1.63	1.6	1.57	1.53	-	-	-	-	-

Table S5. The wavelength of composition fluctuation, d_l and d_m, and crosslink, $d_{x\text{-}link}$, of epoxy resin-tuned samples with m = 0.1.

n	d_l (nm)	d_m (nm)	$d_{x\text{-}link}$ (nm)
0.0	30.59	9.75	2.51
0.1	47.28	10.69	2.59
0.2	51.54	12.20	2.51
0.3	67.34	15.02	2.27
0.4	85.37	17.82	2.15
0.5	184.80	29.64	1.88
0.6	100.37	15.51	1.83
0.7	65.79	15.67	1.75
0.8	45.04	13.65	1.67
0.9	29.64	10.69	1.65
1.0	18.51	8.55	1.65

Table S6. The wavelength of composition fluctuation, d_l and d_m, and crosslink, $d_{x\text{-}link}$, of rubber-tuned samples with m = 0.1.

n	d_l (nm)	d_m (nm)	$d_{x\text{-}link}$ (nm)
0.0	-	-	1.63
0.1	13.72	7.39	1.63
0.2	15.42	7.39	1.63
0.3	19.39	7.74	1.63
0.4	19.93	8.13	1.63
0.5	21.76	8.13	1.65
0.6	18.16	8.13	1.63
0.7	18.05	8.13	1.63
0.8	18.16	8.13	1.63
0.9	18.88	8.13	1.63
1.0	27.12	9.62	1.63

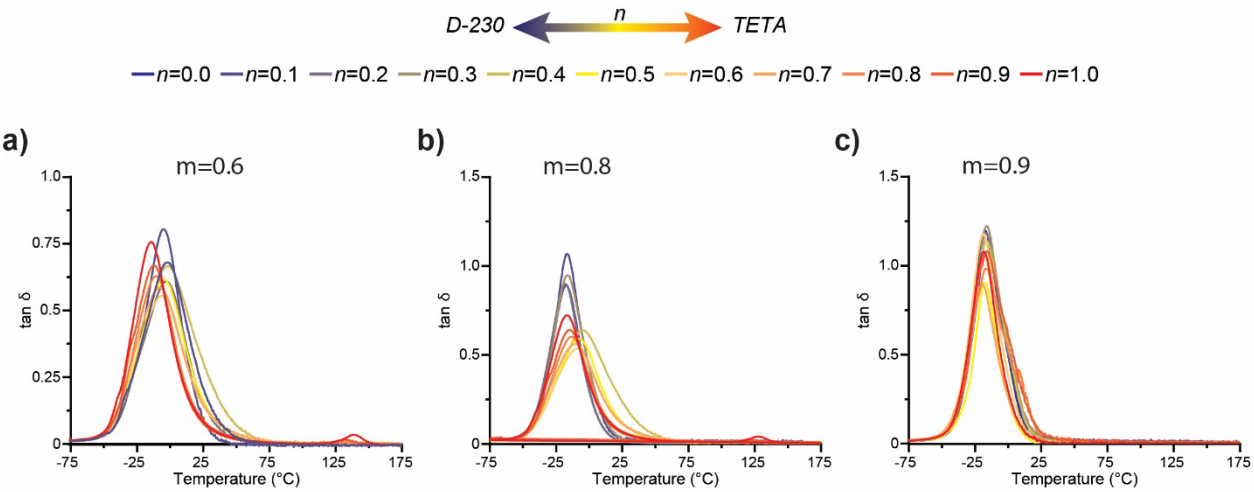

Figure S2. Loss tangent vs. temperature for DGEBA-T3000-TETA-D230 networks formulated with *m*=0.6, 0.8 and 0.9 and varying *n* from 0 to 1 cured at 100°C. For this system, m=[−NH−]$_{0,T3000}$/[−NH−]$_{0,total}$ and n=[−NH−]$_{0,TETA}$/([−NH−]$_{0,TETA}$ + [−NH−]$_{0,D230}$.

1. S. C. Leguizamon, J. Powers, J. Ahn, S. Dickens, S. L. Lee and B. H. Jones, *Macromolecules*, 2021, **54**, 7796–7807.